# 1. Introduction to the Atmosphere and Ocean

J. S. Wright
jswright@tsinghua.edu.cn

## 1.1 Overview

This chapter outlines the main features of the atmosphere–ocean system and motivates the deeper examination to follow. The character of coupled atmosphere–ocean interactions is briefly introduced. Simple energy balance models are derived and used to illustrate the fundamental mechanisms behind variations of temperature with altitude, latitude, and season. The global annual mean energy balance is then presented and briefly discussed.

## 1.2 The Atmosphere–Ocean System

Interactions between the atmosphere and ocean play a fundamental role in determining the state and variability of Earth's climate on all timescales. The atmosphere responds rapidly to regional and global changes in the energy balance, and transmits their influences over large distances. In this way, the atmosphere serves as a bridge, connecting different ocean basins. The ocean has a tremendous capacity to store and release heat (more than 1000 times that of the atmosphere!), which has a remarkable influence on regional climate. For example, the annual range of surface temperature in land-locked Beijing is more than 50°C, while that at the same latitude off the western coast of North America is only about 10°C. The ocean also acts to integrate the effects of synoptic weather disturbances, allowing these short-lived events to influence climate on longer timescales.

Figure 1.1 shows a schematic diagram of the atmosphere–ocean system that illustrates many of the forms that interactions between the atmosphere and ocean take. Heat exchange between the atmosphere and ocean drives global, regional, and local circulations in both the atmosphere and the ocean. Tropical deep convection rapidly transmits the influence of surface conditions to the upper troposphere, where strong winds carry this influence throughout the globe. Wind stress at the ocean surface mixes the upper layer of the ocean and drives surface

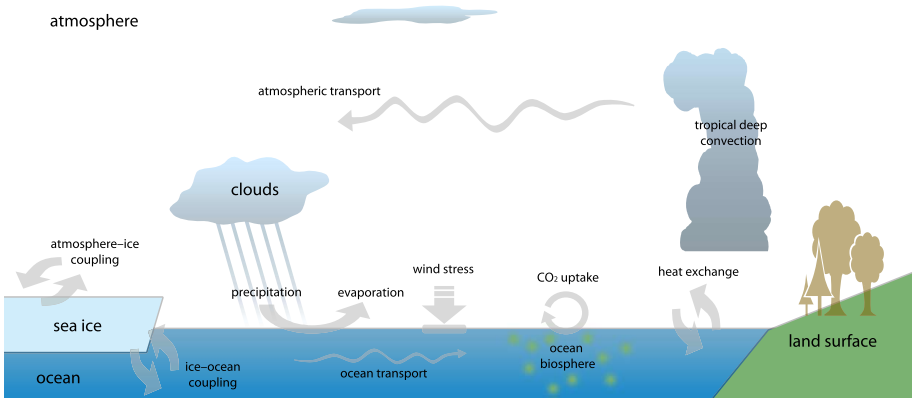


Figure 1.1: Schematic diagram of selected elements in the atmosphere–ocean system.

currents. The depth of this well-mixed upper layer of the ocean (which depends in large part on the magnitude of the wind stress) controls the ocean's response to climate fluctuations at short timescales, while the currents redistribute heat.

The ocean represents the largest reservoir of water on Earth (approximately 97% of the total water supply), and evaporation from the ocean surface provides approximately 90% of the water vapor that eventually becomes rain and snow. The distribution of evaporation and precipitation at the ocean surface creates spatial variations in the salinity (salt content) of surface waters. These variations in salinity contribute in turn to variations in the density of ocean water, which drive vertical motion and mixing within the ocean.

The presence of sea ice fundamentally alters the fluxes of heat and water between the atmosphere and ocean. More than 2% of the world's water currently exists as ice; however, most of this water (more than 99%) is locked up in land ice sheets and permafrost. Although sea ice represents only a tiny fraction of the global volume of ice, its horizontal area is significant. Sea ice introduces additional couplings (ice–atmosphere and ice–ocean) that also play key roles in determining the state, variability, and sensitivity of climate.

The coupled atmosphere–ocean system varies according to several distinctive modes. These modes have substantial implications for global and regional climate and ecological health. The most pronounced mode of coupled atmosphere–ocean variability is the El Niño–Southern Oscillation (ENSO), which is also the largest source of climate variability in the instrumental record. ENSO describes an oscillation of sea surface temperatures and pressures in the tropical Pacific, and is caused by a positive ocean–atmosphere feedback mechanism (**?**). The eastern tropical Pacific is typically much cooler than the western tropical Pacific at the surface. Deep tropical convection preferentially occurs over warmer sea surface temperatures, and is therefore generally concentrated in the western tropical Pacific. During the warm phase of ENSO (El Niño), the eastern tropical Pacific becomes warmer than normal, shifting the location of deep tropical convection toward the east. During the cold phase of ENSO (La Niña), the eastern tropical Pacific becomes cooler than normal, shifting the location of deep tropical

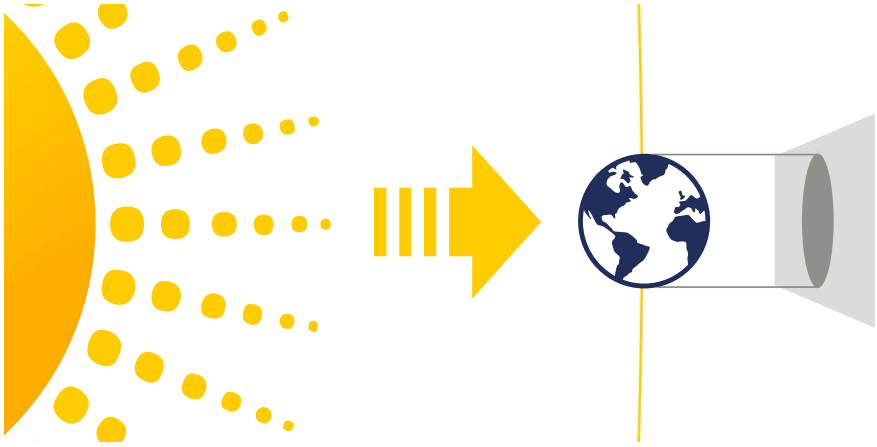

Figure 1.2: Schematic diagram of the flux of solar radiation reaching the Earth. The solar flux is spread out over the entire surface area of the Earth ($4\pi a^2$), but the shadow area is a disc with area $\pi a^2$.

convection further toward the west. The effects of these shifts are felt worldwide. Although the exact impacts of every ENSO event are unique, the warm and cold phases of ENSO often elicit systematic regional responses in surface temperature and precipitation: some regions get colder and some get warmer; some regions get drier and some get wetter. We will examine ENSO and several other major modes of coupled atmosphere–ocean variability in greater detail in the latter half of this course.

## 1.3 An Energy Balance Perspective

The global mean temperature of Earth is remarkably stable in time. This stability indicates that the flux of energy into the Earth system is approximately equal to the flux of energy out of the system. This leads us to the simplest class of climate models: the energy balance model. Although energy balance models represent a gross simplification of the climate system, they nevertheless provide a useful starting point for understanding atmosphere–ocean interactions, which fundamentally depend on the availability and exchange of energy.

### 1.3.1 Solar radiation

The ultimate source of energy to the atmosphere–ocean system is the sun. Observations indicate that the flux of solar energy at the position of the Earth ($S_0$) is approximately $1366\,\mathrm{W\,m^{-2}}$. Only half of the Earth is facing the sun at any given time, so the planet intercepts a disc of solar radiation of area $\pi a^2$, where $a$ is the radius of the planet (on average $6.37 \times 10^6$ m). The surface area of the planet is $4\pi a^2$, so the global mean solar radiation flux is

$$S_0 \frac{\pi a^2}{4\pi a^2} = \frac{S_0}{4} = 342\,\mathrm{W\,m^{-2}} \tag{1.1}$$

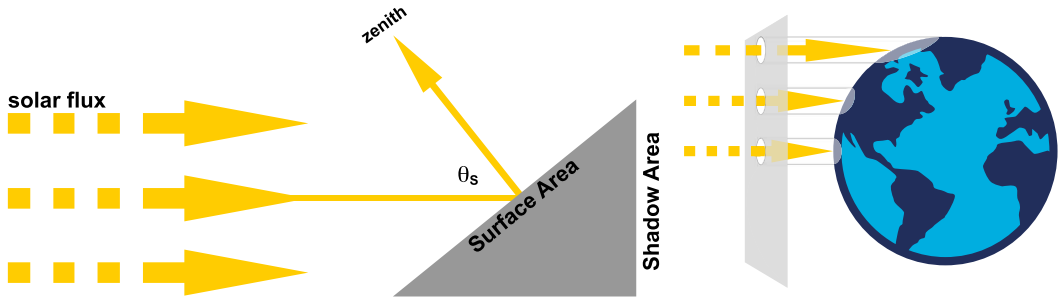


Figure 1.3: Schematic diagrams of the influence of solar zenith angle on solar radiation received.

This quantity is sometimes referred to as $Q$.

The distribution of solar radiation is not uniform over the globe. The distance between the Earth and the sun means that the solar radiation reaching any given location on Earth is very nearly parallel to the solar radiation reaching other locations on Earth. The surface of the Earth is curved; therefore, most of the planet's surface is inclined at an oblique angle to the direction of solar radiation. The solar flux in these locations is therefore spread out over a surface area that is larger than the perpendicular area, as shown in Fig. 1.3. The solar zenith angle varies with latitude, season, and time of day. A larger zenith angle means that the same amount of solar radiation is spread over a larger area. This diffusion of the solar radiation flux with increasing zenith angle is one reason that the tropics are warmer than the polar regions.

Not all of the solar radiation that reaches Earth is absorbed. Some fraction is reflected back into space; this fraction is referred to as the albedo. Figure 1.4 shows the variation of surface and planetary albedo with latitude. The surface albedo represents the fraction of solar radiation reflected by the surface, and varies with surface type (Table 1.1). The ocean absorbs a large fraction of incident solar radiation, so the surface albedo of the ocean is small. Fresh snow reflect a large fraction of solar radiation, so the surface albedo of a region covered with fresh snow has a large albedo. Albedo also varies with solar zenith angle, with a larger solar zenith angle corresponding to a larger albedo. The planetary albedo is the total fraction of sunlight reflected, and can be calculated by dividing the upward solar flux at the top of the atmosphere by the downward solar flux at the top of the atmosphere. Planetary albedo includes the effects of the atmosphere, such as reflection of solar radiation by clouds and aerosols, or absorption of solar radiation by the atmosphere.

Careful examination of Table 1.1 indicates that the global mean albedo should also vary with global mean temperature. For example, the fraction of the Earth covered by ice and snow should be larger during glacial periods (when the global mean temperature is colder), while the fraction of the Earth covered by open ocean should be larger during interglacial periods (when the global mean temperature is warmer). Observations and global climate model simulations suggest that the albedo should vary from about 0.3 (when global mean temperature is warm) to about 0.7 (when global mean temperature is cold). One approach to representing this variation is to model albedo using a hyperbolic tangent function, for example:

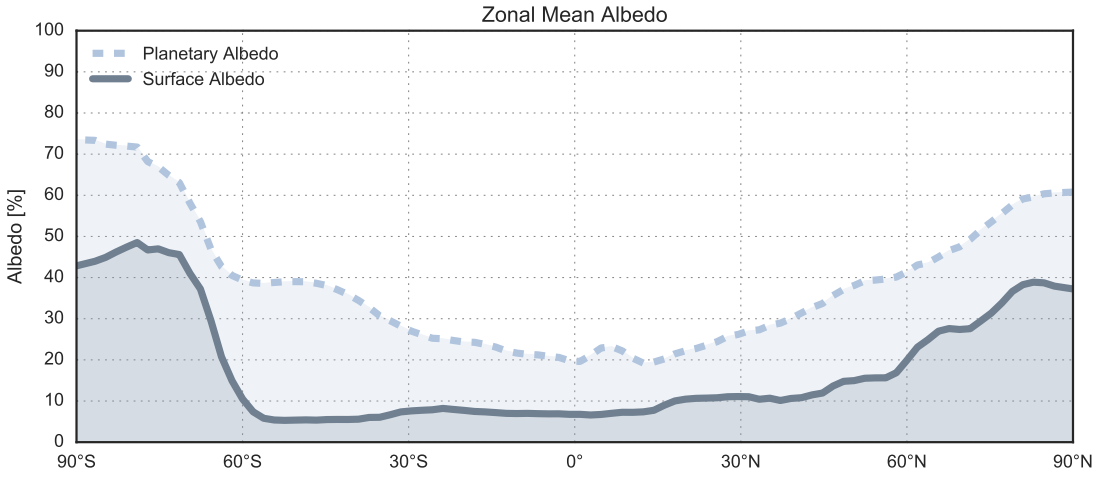


Figure 1.4: The distribution of surface albedo (solid line) and planetary albedo (dashed line) with latitude. Data from the Climate Forecast System Reanalysis.

$$\alpha(T) = 0.5 - 0.2 \tanh\left(\frac{T - 265}{10}\right) \tag{1.2}$$

### 1.3.2 The seasonal cycle

The seasonal variation of the distribution of solar radiation with latitude is determined by the geometry of Earth's orbit (Fig. 1.5). The Earth follows an elliptical orbit around the sun. The closest point to the sun (the perihelion) occurs on approximately 4 January, while the farthest point (the aphelion) occurs on approximately 4 July. The distance between the sun and the Earth at aphelion is $(1+e)\overline{r}$, where $e$ is the eccentricity of the Earth's orbit (currently 0.017) and $\overline{r}$ is the mean distance between the Earth and the sun. Similarly, the distance at perihelion is $(1-e)\overline{r}$. The solar radiation flux received by Earth $S_0$ is inversely proportional to the square of the Earth's distance from the sun:

$$S_0 = \frac{S}{4\pi r^2}, \tag{1.3}$$

where $S$ is the flux of radiation emitted by the sun. Plugging in the changes in sun–Earth distance, the Earth receives 3.3% less solar radiation than average at aphelion and 3.5% more solar radiation than average at perihelion. The total radiation received over the course of a year is therefore largely independent of the eccentricity of the orbit. The eccentricity of Earth's orbit varies over long timescales (100 000–400 000 years) from 0.005 to 0.060. The upper end of this range produces an annual variation in $S_0$ of approximately 20% between perihelion and aphelion.

In the absence of other factors, the seasonal cycle of solar radiation would be determined by the eccentricity of the orbit: summer would occur for the whole globe at perihelion, and

Table 1.1: Albedos for different terrestrial surfaces (from **?**).

| surface | albedo |
|---|---|
| **global mean** | **28–32%** |
| ocean | 2–10% |
| forest | 6–18% |
| grass | 7–25% |
| soil | 10–20% |
| sand | 35–45% |
| ice | 20–70% |
| fresh snow | 70–80% |

winter would occur at aphelion. However, the most important factor in Earth's seasonal cycle is the obliquity of the ecliptic (also known as the angle between the Earth's equatorial plane and its orbital plane) which is currently 23.5°. Boreal (northern hemisphere) summer and austral (southern hemisphere) winter occur when the North Pole is tilted toward the sun. The opposite seasons occur six months later, when the North Pole is tilted away from the sun.

Figure 1.6 shows the influences of both eccentricity and obliquity on the seasonal cycle of solar radiation. The radiation received is greater during austral summer (December–February) than during boreal summer (June–August), indicating the influence of the eccentricity, but the seasonal cycle is dominated by the declination angle of the sun. This angle, shown as a dashed line in Fig. 1.6 is the latitude for which the sun is directly overhead at noon (i.e., the solar zenith angle is zero), and its variation is due to the obliquity. The declination angle of the sun varies from 23.5°S at the boreal winter solstice (December 21–22) to 23.5°N at the boreal summer solstice (June 20–21), and passes through the equator at the vernal and autumnal equinoxes (March 20–21 and September 22–23, respectively). The obliquity varies between a minimum of 22° and a maximum of 24.5° with a period of 41 000 years. These variations have a strong influence on the seasonal and geographic distributions of solar radiation.

The third geometric factor that influences the seasonal cycle is the precession. The longitude of the perihelion precesses by 360° over a period of 21 000 years, so that in about 10 500 years the Earth will be closest to the sun in July and farthest away in January.

The global mean temperature is strongly sensitive to the seasonal cycle. This sensitivity (which arises due to a variety of factors, including atmosphere–ocean feedbacks) means that variations in the orbital parameters over long timescales can exert a strong influence on global climate. Proxy records of past variations in global mean temperature, such as reconstructions of the past 420 000 years using the Vostok ice core, do indeed show significant variations in climate at timescales of 21 000, 41 000, and 100 000 years (**?**). These cycles are called Milankovitch (or Milanković) cycles after the Serbian scientist who first quantified the relationship, Milutan Milanković.

Figure 1.7 shows the annual mean, January, and July variations of solar radiation and surface air temperature with latitude. As in Fig. 1.6, the effect of eccentricity is apparent in the slightly

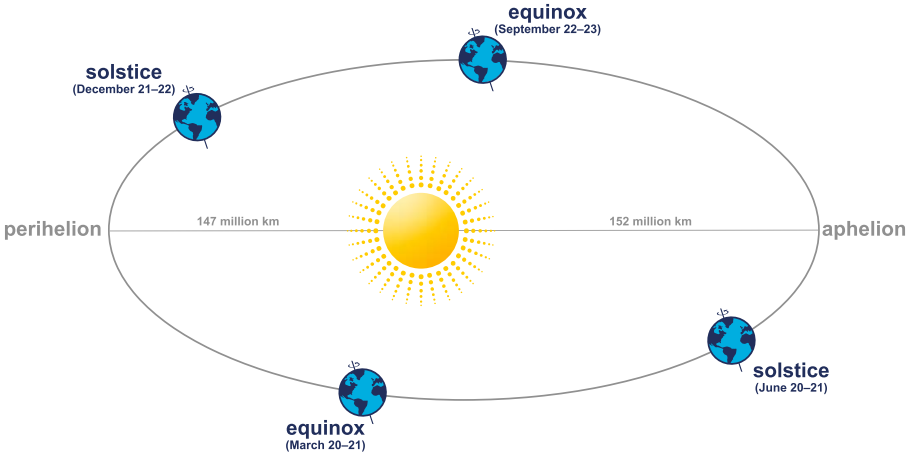


Figure 1.5: Schematic diagram of the Earth's orbit around the sun. The eccentricity is exaggerated.

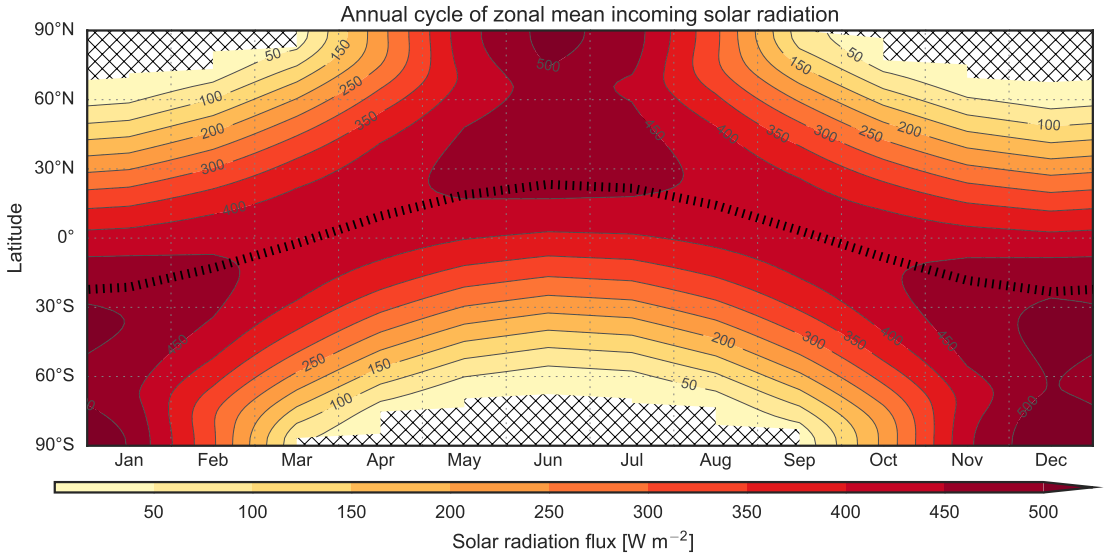


Figure 1.6: The annual cycle of zonal mean solar radiation received at the top of the atmosphere (data from the Climate Forecast System Reanalysis). The dotted line indicates the declination angle of the sun.

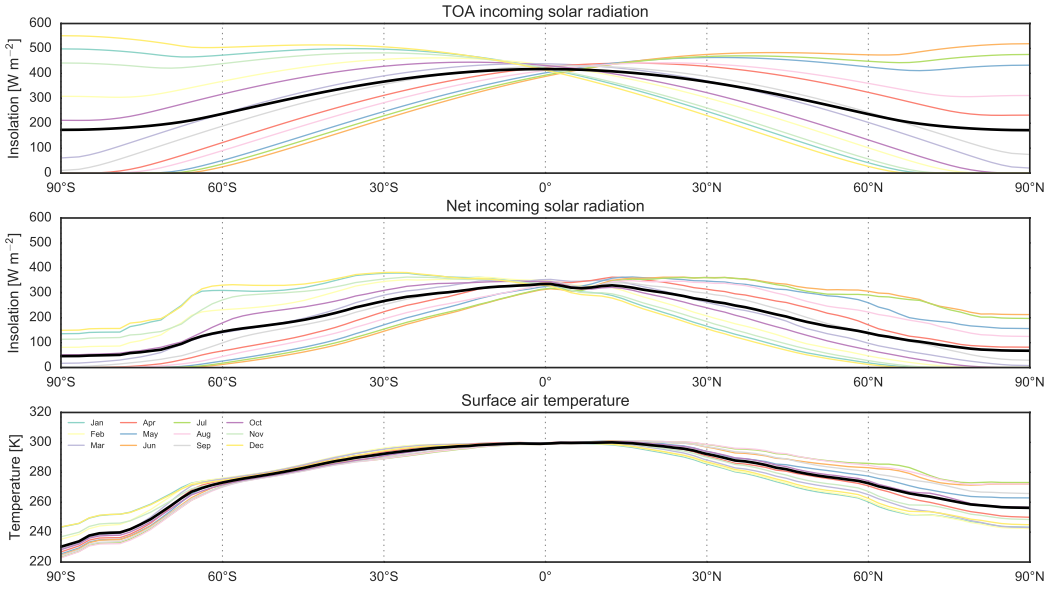


Figure 1.7: Zonal mean total solar radiation received at the TOA (top), net solar radiation (accounting for planetary albedo) entering the atmosphere (center) and surface air temperature (bottom). Annual means are shown in black, along with data from individual months. Data from the Climate Forecast System Reanalysis.

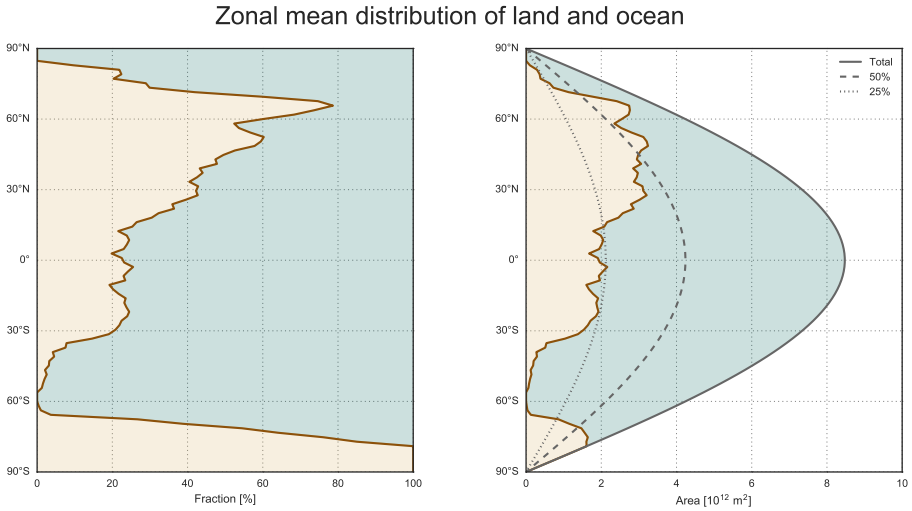


Figure 1.8: The distribution of fractional (left) and total (right) area of land and ocean by latitude. In both panels, the land fraction is to the left of the brown curve and ocean fraction is to the right. The curves in the right panel correspond to 100% (solid), 50% (dashed), and 25% (dotted) of the total area at each latitude.

lower maximum insolation in July relative to January. The distributions of insolation in January is otherwise the mirror image of that in July, but the magnitude and seasonal variation of surface air temperature differ significantly between the northern and southern hemispheres (particularly at high latitudes). These differences arise from differences in the distribution of land and ocean by hemisphere. The area of land is much greater in the northern hemisphere than in the southern hemisphere. Over 80% of the global land area is located in the northern hemisphere. The reduced heat capacity associated with the reduced area of ocean in the northern hemisphere leads to a stronger seasonal cycle (i.e., a stronger variation of surface temperature). Approximately 63% of the global ocean area is located in the southern hemisphere, and the area near 60°S has almost no land cover at all. The hemispheric asymmetry in land and ocean is reversed at high latitudes. The southern hemisphere is occupied by the continent of Antarctica and its massive ice sheet, which keeps surface temperatures extremely cold throughout the year. The northern hemisphere is occupied by the Arctic Ocean. Although much of the surface of the Arctic Ocean is frozen, the ocean itself is connected to the warmer tropics via the large-scale ocean circulation, which keeps the Arctic warmer than the Antarctic for most of the year.

### 1.3.3 The global mean energy balance: An initial guess

The First Law of Thermodynamics states that energy is conserved. More specifically, the change in the system's internal energy must equal the amount of energy entering the system minus the amount of energy leaving the system. Approximately 70% of incoming solar radiation is

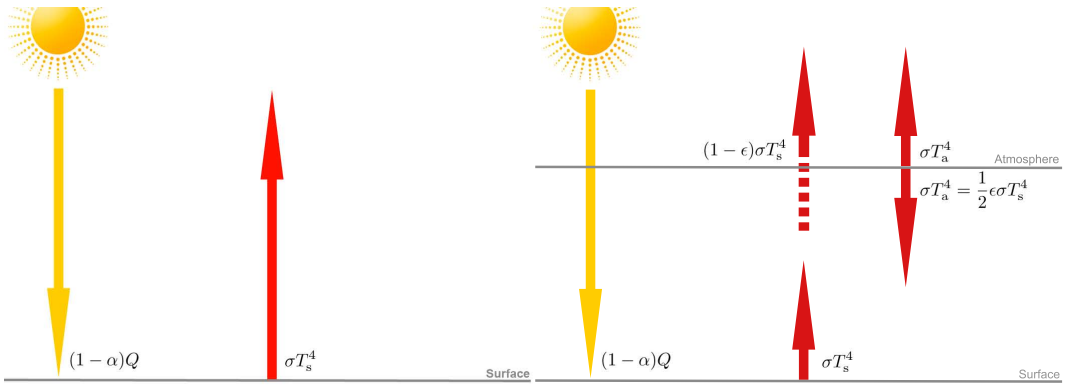


Figure 1.9: The global mean energy budget without (left) and with (right) a single-layer atmosphere that absorbs infrared radiation. The atmosphere is assumed to be transparent to solar radiation. Symbols are defined in the text.

absorbed, yet global mean temperature remains remarkably constant. This constancy implies that the energy gain associated with the absorption of solar radiation must be balanced by an energy loss. This energy loss takes the form of electromagnetic radiation to space.

Stefan's law describes the dependence of total emission from a black body over all wavelengths:

$$E = \sigma T^4 \tag{1.4}$$

where $\sigma = 5.67 \times 10^{-8}\,\mathrm{W\,m^{-2}\,K^{-4}}$ is the Stefan–Boltzmann constant. A black body is a theoretical perfect absorber, which absorbs all incident radiation regardless of wavelength or angle of incidence. Emissivity equals absorptivity for an object in thermal equilibrium, so that a black body is also a perfect emitter. The Earth's emission temperature ($T_e$) is the black body temperature at which the Earth would need to emit radiation so as to balance the incoming flux of solar radiation:

$$\left(\frac{S_0}{4}\right)(1-\alpha) = \sigma T_e^4 \tag{1.5}$$

where $\alpha$ is the global mean albedo. Plugging in $\alpha = 0.3$ and $S_0 = 1366\,\mathrm{W\,m^{-2}}$, the emission temperature can be calculated as 255 K (−18°C).

This first order energy balance (Fig. 1.9, left panel) represents the simplest possible climate model; however, its results are not particularly relevant to life at the surface of the Earth. The mean temperature of the Earth's surface is 288 K (15°C), considerably warmer than the emission temperature. This discrepancy indicates that our description of the energy balance is incomplete.

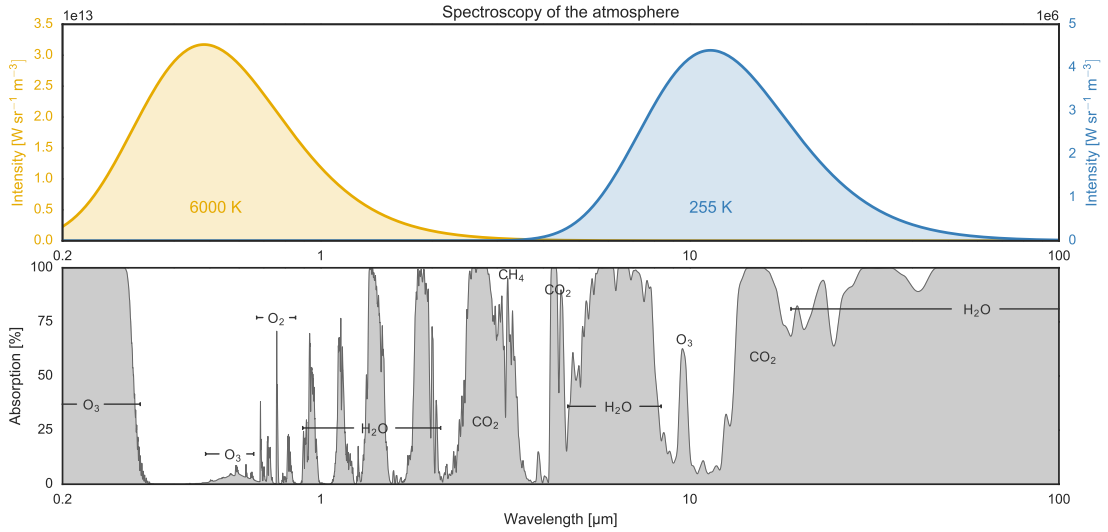


Figure 1.10: (top) Approximate black body emission as a function of wavelength for the sun (6000 K) and the Earth (255 K); (bottom) absorption of radiation by the Earth's atmosphere (data based on HITRAN and provided by Tong Li).

### 1.3.4 The greenhouse effect

The wavelength of maximum radiation for the emission temperature can be calculated using the Wien displacement equation:

$$\lambda_{\max} T_e = 2897 \mu\text{m K} \tag{1.6}$$

With $T_e = 255$ K, $\lambda_{\max}$ is approximately 11 μm.

Figure 1.10 shows approximate black body curves for the sun and the Earth, along with the wavelength dependence of absorption by Earth's atmosphere. Both carbon dioxide ($CO_2$) and water vapor ($H_2O$) have strong absorption bands near 11 μm. The presence of water in particular leads to strong absorption and re-emission of outgoing infrared radiation (Fig. 1.10, bottom panel). Absorption by the atmosphere results in multi-directional re-emission. Assuming a plane atmosphere located above a plane surface and perpendicular to the incoming flux of solar radiation (Fig. 1.9, right panel), only half of atmospheric re-emission is directed toward space. The other half is directed back toward the surface, increasing the energy flux at the surface. The surface must then warm to balance the increased downward energy flux, resulting in a surface temperature $T_s$ that is greater than the emission temperature $T_e$.

The inclusion of the greenhouse effect changes the energy balance model. If the atmosphere is a perfect absorber of the radiation emitted by the surface, then the energy balance is still described by Eq. 1.5, but with $T_e$ representing the atmospheric emission temperature rather than the surface temperature. However, examination of Fig. 1.10 reveals gaps in atmospheric absorption of long-wave radiation, particularly around the 11 μm maximum for emission

from the surface. Radiation in this part of the spectrum can escape directly to space, without absorption and re-emission by the atmosphere. This suggests the more complex energy balance

$$\left(\frac{S_0}{4}\right)(1-\alpha) = (1-\epsilon)\sigma T_s^4 + \sigma T_a^4 \tag{1.7}$$

where $\epsilon$ represents the fraction of outgoing radiation from the surface absorbed by the atmosphere ($0 \le \epsilon \le 1$) and $T_a$ is the temperature of the atmosphere. Because the atmosphere re-emits equally toward space and toward the surface, and because the energy emitted by the atmosphere must equal the energy absorbed by the atmosphere

$$\sigma T_a^4 = \frac{1}{2}\epsilon\sigma T_s^4. \tag{1.8}$$

The energy coming into the Earth system in the form of solar radiation must still be balanced by the energy going out, so that

$$\sigma T_e^4 = (1-\epsilon)\sigma T_s^4 + \frac{1}{2}\epsilon\sigma T_s^4 = (1-\frac{1}{2}\epsilon)\sigma T_s^4. \tag{1.9}$$

**?** proposed an alternative approach to estimating the dependence of outgoing energy on surface temperature. Budyko's approach relies on an empirical fit to observations of global mean temperature and energy fluxes (as opposed to a theoretical derivation based on Stefan's law and the assumption that Earth can be treated as a blackbody). The general form of this empirical equation is

$$E_{out}(T) = A + B(T - 273.15) \tag{1.10}$$

where $A$ and $B$ are fitting parameters. Budyko's original formulation also included an additional "cloudiness" term. Fits to satellite estimates indicate that $A \approx 203.3\,\mathrm{W\,m^{-2}}$ and $B \approx 2.09\,\mathrm{W\,m^{-2}\,{}^{\circ}C^{-1}}$ (**?**).

The simple conceptual model shown in the right panel of Fig. 1.9 is a useful starting point; however, the real atmosphere is not a single layer but a continuous fluid. In practice, climate modelers must compromise and represent the atmosphere as a series of thin layers, all stacked atop each other. Figure 1.11 shows the radiation budget of such a thin layer of atmosphere. The flux of solar radiation $E$ entering the top of the layer is attenuated by an amount $\Delta E$ due to absorption of solar radiation within the layer. Similarly, the upward flux of long-wave radiation $L_u$ from the surface and lower levels of the atmosphere is attenuated by an amount $\Delta L_u$ by long-wave absorption within the layer. We must also consider the downward flux of long-wave radiation $L_d$ from higher levels of the atmosphere, which is attenuated by an amount $\Delta L_d$. These energy inputs must be balanced by the emission of long-wave radiation plus changes in the temperature of the layer:

$$mc_p\frac{dT}{dt} = \Delta E + \Delta L_u + \Delta L_d - 2L_e \tag{1.11}$$

where $m$ is the mass of the layer and $c_p$ is the specific heat of air at constant pressure.

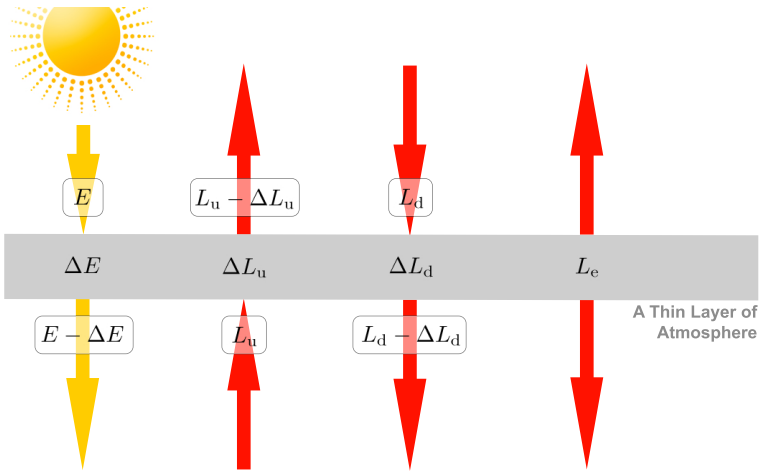


Figure 1.11: Radiation budget of a thin layer of atmosphere.

It is also useful to consider the thermal inertia of the entire atmosphere, which provides an indication of how quickly the atmosphere responds to a climate forcing. Suppose that the atmosphere, which is initially in thermal equilibrium, is suddenly heated by a one-time increment $\Delta T_0 \ll T_e$. The atmosphere is then no longer in equilibrium, as the energy emitted as outgoing long-wave radiation now exceeds the energy received from the sun. The rate of temperature change following the sudden heating is

$$Mc_p \frac{dT}{dt} = -\sigma(T_e + \Delta T)^4 + \frac{S_0}{4}(1-\alpha) \tag{1.12}$$

where $M$ is the mass of the atmosphere per unit area. Substituting from equation 1.5 gives

$$Mc_p \frac{dT}{dt} = -\sigma T_e^4 (1 + \frac{\Delta T}{T_e})^4 + \sigma T_e^4. \tag{1.13}$$

Expanding and removing higher order terms yields

$$Mc_p \frac{dT}{dt} = -\sigma T_e^4 \frac{4\Delta T}{T_e}. \tag{1.14}$$

Note that $T = T_e + \Delta T$, where $T_e$ is independent of time, so

$$\frac{d\Delta T}{dt} = -\left(\frac{4\sigma T_e^3}{Mc_p}\right)\Delta T \tag{1.15}$$

This equation has the solution

$$\Delta T(t) = \Delta T_0 e^{(-t/\tau)} \tag{1.16}$$

where $\Delta T_0$ is the initial perturbation to atmospheric temperature and $\tau$ is the radiative relaxation time constant:

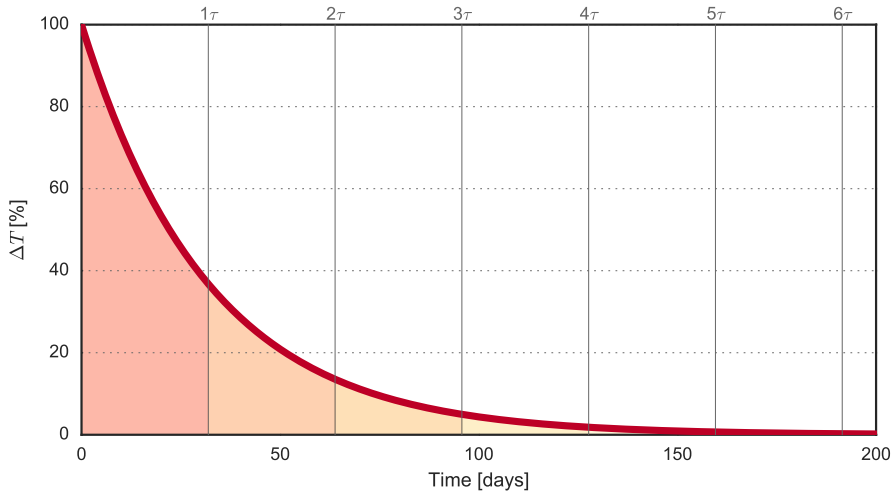


Figure 1.12: Analytical solution to Eq. 1.16 for arbitrary $\Delta T_0$.

$$\tau = \frac{Mc_p}{4\sigma T_e^3} \tag{1.17}$$

For Earth's atmosphere, $M = 10.328 \times 10^3\,\mathrm{kg\,m^{-2}}$ and $c_p = 1004\,\mathrm{J\,kg^{-1}\,K^{-1}}$, so that $\tau$ is approximately 32 days. The temperature perturbation will therefore be reduced by a factor $e^{-1}$ every 32 days. For an initial perturbation $\Delta T_0 = 1\,\mathrm{K}$, the temperature perturbation would be 0.37 K after 32 days, 0.13 K after 64 days, and 0.05 K after 96 days. Almost the entire temperature perturbation would be erased by long-wave cooling within 100 days.

The results of this calculation suggest that the atmosphere does not respond significantly to daily variations in solar radiation, because the radiative relaxation time constant $\tau$ is much longer than a day. By contrast, the atmosphere does respond significantly to seasonal variations in solar radiation, or variations associated with volcanic eruptions (which can alter the radiative balance for several years).

### 1.3.5 The global mean energy balance revisited

By combining satellite observations of radiative fluxes at the top of the atmosphere with increasingly sophisticated models of radiative transfer, it is possible to calculate the energy budget of the Earth–atmosphere system. At the top of the atmosphere, the global mean flux of incoming solar radiation is balanced in part by outgoing long-wave radiation from the surface and atmosphere, with the remainder made up by the reflection of approximately 30% of the solar radiation. The surface and atmospheric energy budgets consist primarily of absorbed solar and long-wave radiation balanced predominantly by long-wave emission. The radiative exchange of energy between the surface and the atmosphere does not strictly balance, however, with the surface receiving more energy than it emits and the atmosphere emitting more energy

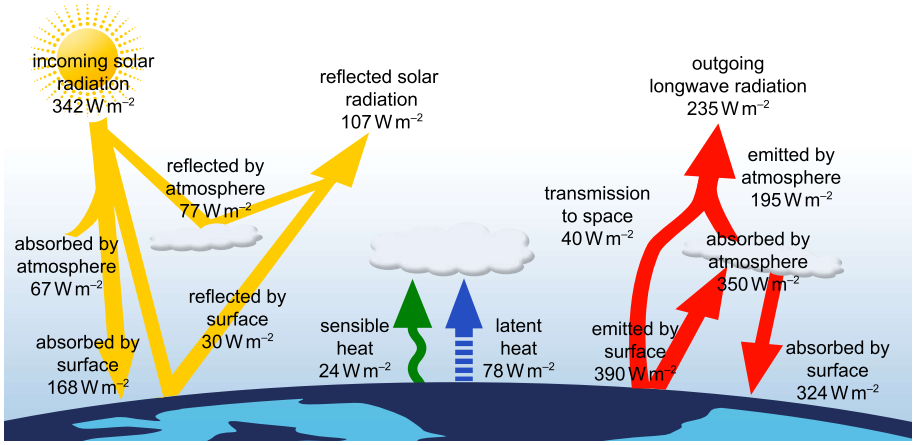


Figure 1.13: The global mean annual mean radiation budget. Adapted from **?**.

than it receives. This energy imbalance is closed by the inclusion of fluxes of sensible heat and latent heat directed from the surface to the atmosphere. Sensible heat is the direct exchange of heat between the surface and the lowest layer of the atmosphere, which is then mixed into the atmosphere by turbulence. Latent heat represents the exchange of energy associated with the evaporation of water from the surface, which then transfers energy to the atmosphere during condensation and precipitation. We will return to these concepts in future chapters.

### 1.3.6 Horizontal diffusion

Up to this point, our energy balance models have only considered vertical fluxes of energy. The atmosphere and ocean are fluids, and the winds and currents in these fluids are capable of rapidly transporting heat in the horizontal direction.

The upper left panel of Fig. 1.14 shows the distributions of solar radiation absorbed by the Earth–atmosphere system (i.e., incoming solar reduced by the planetary albedo) and outgoing long-wave radiation by latitude at the top of the atmosphere. Absorbed solar radiation is greater than outgoing long-wave radiation in the tropics (between approximately 35°S and 35°N), but is less than outgoing long-wave radiation in the extratropics (poleward of approximately 35°). The magnitude of the outgoing long-wave radiation indicates the emission temperature. Emission temperatures are cooler than expected in the tropics (based on absorbed solar radiation) and warmer than expected in the extratropics. These differences indicate a horizontal redistribution of energy by fluid motion within the atmosphere and ocean. The magnitude of this horizontal energy transport is shown in the lower left panel of Fig. 1.14. This energy transport is calculated by integrating the difference between outgoing long-wave radiation and absorbed solar radiation from the north pole to the south pole, and is positive for northward transport. Energy transport is poleward throughout both hemispheres. Calculations indicate that the atmosphere and ocean each account for approximately half of the poleward energy transport (**?**).

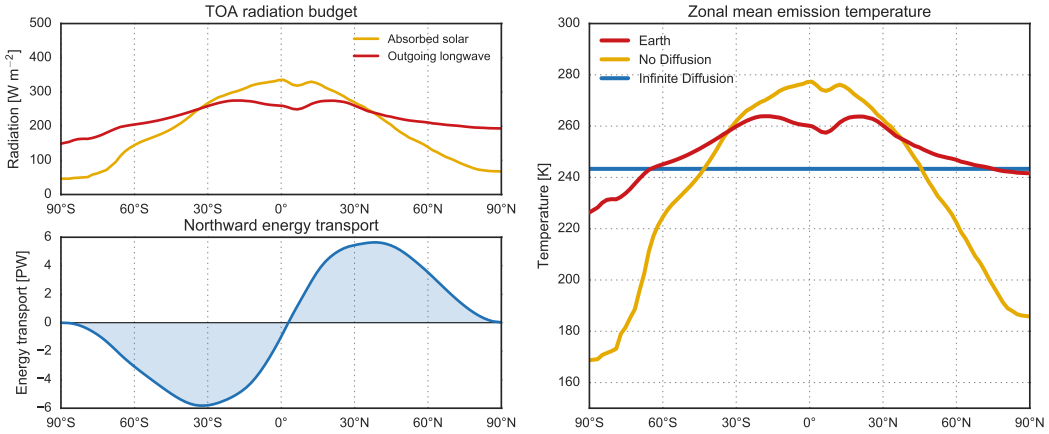


Figure 1.14: Upper left: zonal mean net incoming solar radiation (yellow) and outgoing long wave radiation (red) at the top of the atmosphere (TOA). Lower left: annual mean zonal mean northward energy transport in the atmosphere and ocean inferred from the TOA energy balance. Right: zonal mean emission temperature ($T_e$) based on absorbed solar radiation assuming no diffusion by the atmosphere and ocean (yellow), infinite diffusion (blue), and observed outgoing long wave radiation (red). Data from the Climate Forecast System Reanalysis.

The right panel of Fig. 1.14 depicts the expected emission temperature in a variety of scenarios. The first scenario (red) represents a situation with no diffusion (i.e., outgoing long-wave radiation balances absorbed solar radiation everywhere). This scenario could correspond to a planet with no ocean and no atmosphere, and with zero thermal conduction through the surface. The second scenario (blue) represents a situation with infinite diffusion (i.e., the emission temperature is the same everywhere). The final scenario (black) corresponds to the Earth. Horizontal energy transport by the atmosphere and ocean is clearly an important component of the Earth's energy balance. In reality, this energy transport is accomplished primarily by winds and currents rather than diffusion. However, diffusion is often used as a computationally efficient representation of transport in energy balance models, which are necessarily heavily simplified.